Electrochemical Growth of Metallic Nanoparticles onto Immobilized Polymer Brush Ionic Liquid as a Hybrid Electrocatalyst for the Hydrogen Evolution Reaction

Thuan-Nguyen Pham-Truong, Ouiza Mebarki, Christine Ranjan, Hyacinthe Randriamahazaka, Jalal Ghilane

Electrochemical Growth of Metallic Nanoparticles onto Immobilized Polymer Brush Ionic Liquid as a Hybrid Electrocatalyst for the Hydrogen Evolution Reaction

Thuan-Nguyen Pham-Truong, Ouiza Mebarki, Christine Ranjan, Hyacinthe Randriamahazaka and Jalal Ghilane*

Université de Paris, ITODYS, CNRS, UMR 7086, SIELE group 15 rue J-A de Baïf, F-75013 Paris, France.

ABSTRACT: Platinum and palladium are the first choice electrocatalysts to drive the hydrogen evolution reaction. In this report, surface modification was introduced as a potential approach to generate hybrid electrocatalyst. The immobilized polymer brush, poly(1-allyl-3-methylimidazolium) (PAMI), was used as a nanostructured template for guiding the electrochemical deposition of metallic nanoparticles (Pd, Pt). The intrinsic properties of the polymer brush in term of nanostructured architecture and the anions mobility within the polymer was exploited to generate a hybrid electrocatalyst. The latter was generated using two different approaches including the direct electrochemical deposition of Pd or Pt metal and the indirect approach through the anion exchange reaction followed by the electrochemical deposition under self-electrolytic conditions. The hybrid structure based on the polymer/metallic NP exhibits an enhancement of the catalytic performance toward hydrogen evolution reaction with a low Tafel slope and overpotential. Interestingly, the indirect approach leads to decrease the metal loading by two orders of magnitude, when compared to those generated in the absence of the polymeric layer, while retaining the electrocatalytic performance.

■ INTRODUCTION

In the era that sustainable sources become considerable for supplying the continuous increase of energetic demand, efficient catalysts are strongly required to boost the current conversion and storage systems up to higher performance. Hydrogen and oxygen are being classed as principle input and key component into several clean energy technologies[1-5]. Energy conversion through hydrogen evolution reaction (HER) is considered as a promising sustainable pathway to produce hydrogen. In order to efficiently drive this reaction appropriates catalysts are essential. The state-of-the-art of hydrogen evolution reaction covers three families of catalysts resulting from noble metals and alloys[6-10], non-noble metals or transition metals[11-13] and metal-free catalysts based on all-carbon materials[14-17]. Accordingly, despite the high cost and low abundance, noble metals-based materials, platinum and palladium, are still largely used as highly efficient catalysts.[1,18,19] In the literature, two strategies were developed to overcome the cost-effective noble metal catalyst including the identification of promising non noble metal catalysts,[20,21] or seeking for a new methods to lower the quantity of noble catalysts while retaining the catalytic performances. Relying on advantageous performance offered by the noble materials, nanosized structures have been investigated and exhibit an increase of the catalytic activity concomitant with a decrease of the required quantity of material.[22,23] The nanosized catalysts are generated using several approaches including chemical synthesis, electrochemical deposition, etc.[24-26] In this context, tailoring the physical-chemical properties at the molecular/atomic level becomes crucial not only for boosting the performance of the existing materials but also for creating new type of molecular entities for storing and releasing the energy. Thus, very small amount of Pt nanoparticle is found to be able for boosting the system up to commercial Pt/C.[24] However, the deposition of Pt depends strongly on the chemical composition, crystalline structure and morphology of the substrate.

Besides that, ionic liquids (ILs) become one of the best candidates for settling the energetic problems.[27,28] This family of compounds is nowadays a major research field offering relevant ability in different applications.[29] Interestingly, an infinity of ionic liquids can be obtained resulting from the possibility to tailor the physical-chemical properties at (sub)nanoscopic scale.[30] Taking the advantage of the ionic liquids, one of the promising approaches in the electrocatalysis field is the marriage of the metal catalyst and the ionic liquid. For example, several works report the use of ionic liquids as media for the synthesis of electrocatalysts leading to a higher performance toward the oxygen and hydrogen evolution reactions (OER and HER).[31-33] Besides that, Pt catalyst covered with ionic liquid has been investigated, displaying enhanced perfor-

mance toward OER and oxygen reduction reactions ORR.[34,35] However, the nature of the interaction between the catalyst and the ionic liquid are not well defined and less attention has been paid to the investigation of ionic liquid modified noble metal for HER. Therefore, the capability to tune the chemical properties of ionic liquids could lead to the rational design of an attractive class of effective catalysts based on Pt and Pd modified ionic liquid.

In our previous study, we demonstrate that immobilized polymeric brush based ionic liquid, covalently attached to the carbon electrode, acts as an efficient electrocatalyst toward the oxygen reduction reaction.[36] In addition, the polymer ionic liquid, poly(IL), was successfully used as a platform for the host guesting of other materials (Pt, Au and carbon dots) providing a synergetic effect to the hybrid structure toward ORR.[36,37] Even though the increase of the catalytic activity of the as-prepared substrates, the interface between the ionic liquid moieties and the particles is relatively vague. In this current investigation, the poly(IL) is used as a nanostructured platform for guiding the electrochemical deposition of metallic nanoparticles. The immobilized poly(1-allyl-3-methylimidazolium) (PAMI) is prepared by means of surface-initiated atom transfer radical polymerization as reported in our previous works.[36] Being known as the best candidate for hydrogen evolution reaction, noble metals were used, including palladium and platinum. Next, the electrochemical deposition of metal onto GC/PAMI has been performed via two distinct approaches labeled direct and indirect electrodeposition process (Scheme 1). The direct approach consists on performing the electrochemical deposition of Pt or Pd over GG/PAMI. While the indirect approach involves the anion exchange property of the polymeric ionic liquid allowing the incorporation of metal-based anions (XCl_4^{2-}, X = Pt, Pd) followed by the electrochemical deposition in electrolyte free solution (Scheme 1).

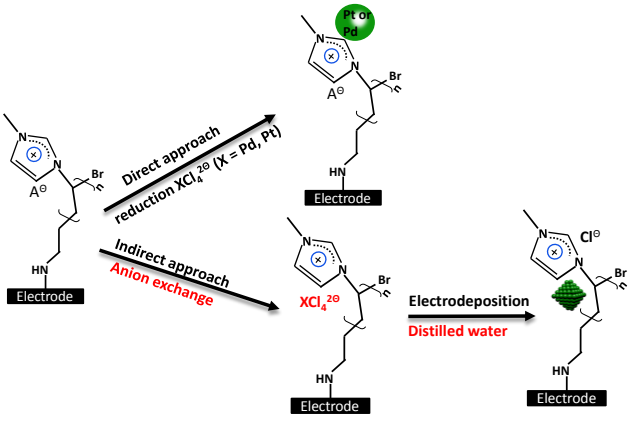

Scheme 1. Two different approaches for electrochemical deposition of nanoparticles onto GC/PAMI substrates. Direct electrochemical deposition of NPs and indirect pathway through ion exchange step.

■ EXPERIMENTAL SECTION

Instrumentation. All the electrochemical measurements were performed using three–electrode setup, where stainless steel mesh and saturated calomel electrode (SCE) were used as counter and reference electrodes, respectively. Electrochemical impedance spectroscopy EIS measurements are performed by a VSP (Bio-logic), the remaining electrochemical measurements were recorded with a CHI900C (CH Instrument, Austin, Texas). For hydrogen evolution reaction, 0.5 M of sulfuric acid (Sigma Aldrich, > 95%) was used and bubbled with highly purified Argon (Air Liquide, France) for 30 minutes. During the tests, the as-prepared solution was kept under inert atmosphere. All the potentials were converted versus a reversible hydrogen electrode (RHE) via the following equation (1):

$$E\ (V/RHE) = E\ (V/SCE) + 0.241 + 0.059\ pH \quad (1)$$

The morphology of the prepared films was recorded by SEM (Zeiss SUPRA 40). The elemental composition at the extreme surface was characterized via X-ray photoelectron spectroscopy using Thermo VG Scientific ESCALAB 250 system fitted with a microfocused, monochromatic Al Kα (hν = 1486.6 eV) 200 W X-ray source.

Preparation of the polymer PAMI modified electrodes. The used working electrodes are glassy carbon or Indium-Tin Oxide (ITO) (ITOSOL12, 8-12 ohms with a thickness of 370 nm on 1.1 mm of glass, supplied by Solems, France). The polymerization was performed following our previously reported procedure[36]. Briefly, the polymerization is based on a two-step process. The first step is the immobilization of initiator layer through the electrochemical oxidative grafting of primary amine, 2-bromoethylamine, yielding to a bromide terminated electrode. Next, the modified electrode was immersed in a solution containing 10 mM of the ionic liquid monomer, 1-allyl-3-methylimidazolium bromide, and a catalytic amount of all the necessary reagents (CuCl, $CuCl_2$ and N,N,N′,N′′,N′′-Pentamethyldiethylenetriamine as activator, deactivator and complexing agent, respectively) (Figure S1). After keeping the polymerization for 2 hrs at 60°C and under inert atmosphere, the electrodes were removed from the solution and were successively rinsed with distilled water, acetone and acetonitrile. Finally, the electrodes were dried under Argon stream.

Electrodeposition of Pd and Pt via a direct approach. The metallic nanoparticles were deposited onto the electrode surface, GC/Poly(IL), by chronoamperometry technique, which consists to apply a fixed potential during 100 s in deoxygenated 1 mM of metallic salt, i.e. Na_2PdCl_4 (Sigma Aldrich, > 99.9%) or K_2PtCl_4 (Sigma Aldrich, >99.9%) aqueous solution containing 0.1 M of KCl (Bioreagent, Sigma Aldrich, > 99%) as supporting electrolyte. The applied potential is ranged from 0.2 to -1 V/SCE for Pd deposition and from 0 to -1 V/SCE for Pt deposition. The generated electrodes were rinsed thoroughly with distilled water (<18 MΩ.cm), ethanol (GRP RECTAPUR, 96%) and dried under Argon stream.

Electrodeposition of Pd via an indirect approach. After the polymerization, the electrode was immersed in aqueous solution containing a 1 mM of metallic salt (Na_2PdCl_4) during 2h. Next, the electrode was rinsed thoroughly with distilled water and transferred into the electrochemical cell containing ultrapure water (>18 MΩ.cm)

without the addition of the supporting electrolyte. The electrodeposition was performed under similar potential range, as described above. Then, the modified electrodes were rinsed with distilled water, ethanol and dried under Argon stream.

■ RESULTS AND DISCUSSION

Direct electrochemical deposition approach.

The electrochemical deposition of palladium and platinum was performed directly on GG/Poly(IL) electrode in electrolytic solution containing 1 mM of the corresponding metallic salt. To cover a large window of deposition potential, different samples were prepared with a deposition potential ranging from 0.2 to -1 V/SCE at a fixed time (100 s). The typical electrochemical response of Pd decorated GC/PAMI electrode was recorded in N_2-saturated 0.5 M H_2SO_4 solution as shown in Figure S2. At a potential higher than 0.7 V, an anodic peak is observed corresponding to the oxidation of Pd. These oxidized species are reduced at 0.4 V. Besides that, the reduction peak at the potential ranging from 0 V to -0.4 V corresponds to the proton reduction/hydrogen adsorption and the reverse peak attributed to hydrogen evolution/desorption process. Similar CV's for Pt decorated GC/Poly(IL) was also recorded showing the transformation of metallic platinum into oxide at 1.3 V and the reverse reaction is observed at 1.2 V. Even though the hydrogen adsorption peak is hindered by the HER, the anodic peak indicates a strong desorption of the H_2 molecule from the Pt surface. Depending on the applied potential, the nucleation and growth process of the metallic structure at the GC/Poly(IL) are different, resulting from the difference of the thermodynamic barrier. These electrochemical characterizations confirm the electrodeposition of Pd and Pt over the GC/Poly(IL) electrode.

Scanning Electron Microscopy (SEM) leads to determine the morphology and the size of the deposited materials. Typical images of the samples prepared by depositing Pd or Pt on GC/Poly(IL) electrodes are presented in the Figure 1.

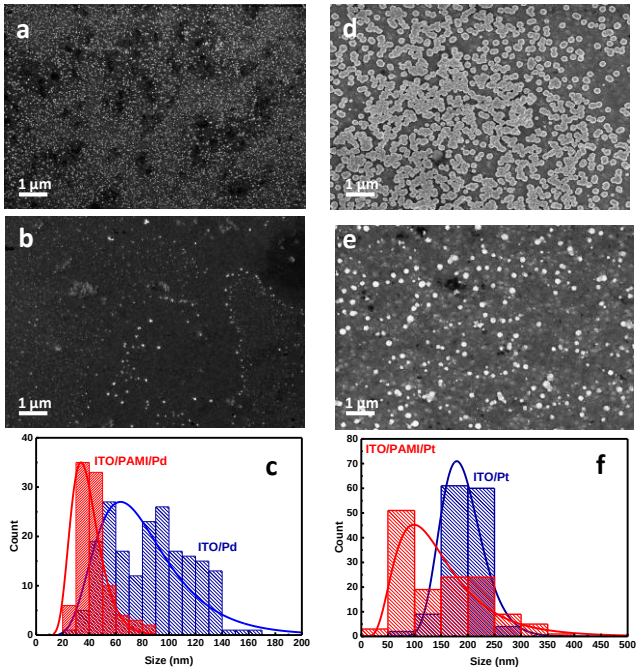

Figure 1. SEM images of (a) ITO/Pd NPs deposited at -0.2 V/ SCE and (b) ITO/Poly(IL)/Pd NPs; (c) Pd NPs size distribution in the presence and in the absence of Poly(IL) layer; (d) ITO/Pt NPs deposited at -0.6 V/ SCE; (e) ITO/Poly(IL)/Pt NPs; (f) Pt NPs size distribution.

The SEM revealed that the morphology and the size of the particles deposited onto ITO are different depending on the presence or the absence of the polymeric ionic liquid layer. Common behavior for both metals is the formation of nanoparticles after the electrochemical deposition. The size of the particles decreases in the presence of the poly(IL) layer. For Pd NPs deposited onto ITO a very dense nanoparticles layer cover the electrode with a larger size (up to 200 nm) were obtained as shown in Figure 1a, while in the presence of the Poly(IL) layer less dense NP layer is observed and the particles size is smaller than those obtained in the absence of the polymer brush layer (< 50 nm) (Figure 1.b). In the case of the platinum electrodeposition, smaller nanoparticles were observed in the presence of the PAMI (Figure 1e) when compared to those generated on ITO electrode (Figure 1d). Figure 1c and f compare the nanoparticles size distribution and confirm that in the presence of the polymer brush structure the Pt and Pd NPs have an average size of about 50 nm while in the absence of the poly(IL) the NPs size reach an average of about 200nm. By depositing metallic nanoparticles via chronoamperometry technique, the measured current is composed of 3 components, including the double layer charge contribution, the 2D-instantaneous nucleation and 3D nucleation with diffusion-controlled growth. From the SEM images, the formation of 3D nanoparticles was observed. Consequently, the measured current, especially the nucleation rate constant varies with the applied potential resulting from the mechanism of Langmuir – type adsorption/desorption equilibrium followed by 3D nucleation under diffusion-controlled regime.[38-40] Even though the mechanistic investigation of nucleation and growth of the

nanoparticles is still at the spectacular stage, it is still possible to conclude that the nucleation of nanoparticles is strongly affected by the concentration of the metallic ions at the vicinity of the electrode surface and the applied potential. By combining the SEM images and the polymer brushes structure, possible explanation can be assigned to the high density of cations within the film that are converted to numerous nucleation sites for the formation of the final material. Consequently, smaller size particles are obtained using the poly(IL) as template, i.e. higher specific surface area, rather than big particles in the absence of the poly(IL) film.

X-ray photoelectron spectroscopy (XPS) was used to follow the change in the atomic composition of the surfaces ITO/Poly(IL)/Pd NPs and ITO/Poly(IL)/Pt NPs.

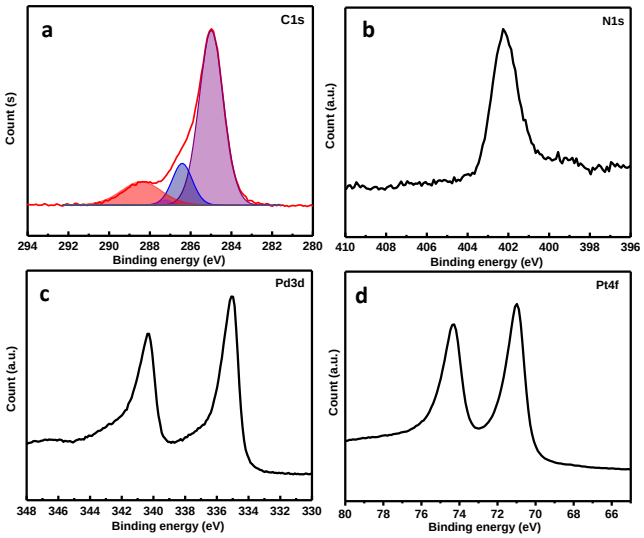

Figure 2. (a), (b) and (c) XPS high resolution spectra of C(1s), N(1s) and Pd(3d) recorded on ITO/Poly(IL)/Pd. (d) XPS spectrum of Pt for the sample ITO/Poly(IL)/Pt.

Figures 2a and b display the high-resolution spectra of C(1s) and N(1s) elements. Similar behavior was observed for both surfaces despite the presence of the Pd or Pt NPs. The C(1s) spectrum exhibits the presence of three components at binding energy of 285, 286.4 and 288.4 eV which are attributed to the binding energy of carbon backbone (C–C), –C=N group from imidazolium ring and –COO from the surface contamination, respectively.[41] Besides that, the N(1s) spectra displays a major signal at 401.7 eV corresponding to imine group from imidazolium ring.[42] These results confirm the presence of the poly(IL), PAMI, at the electrode surface. In addition, the XPS spectrum shown in Figure 2 c, reveals the presence of the peak at 335 eV attributed to $Pd3d_{5/2}$ and confirms the presence of metallic Pd.[43] In the case of Pt electrodeposition, the XPS spectrum shows the presence of metallic Pt as attested by the location of the $Pt4f_{7/2}$ peak at 71 eV.[44] The XPS analysis confirms the presence of the poly(IL) and the metallic character of the electrodeposited Pd and Pt NPs.

The electrocatalytic performance of the generated materials toward hydrogen evolution reaction (HER) was evaluated. The selected samples are prepared at different deposition potential ranging from 0.2 V to -1 V/SCE. Figure 3a displays the LSV polarization curves recorded in N_2–saturated 0.5 M H_2SO_4 for Pd deposited onto GC/PAMI at different potentials 0.2, -0.2, -0.4 and -0.8 V/SCE.

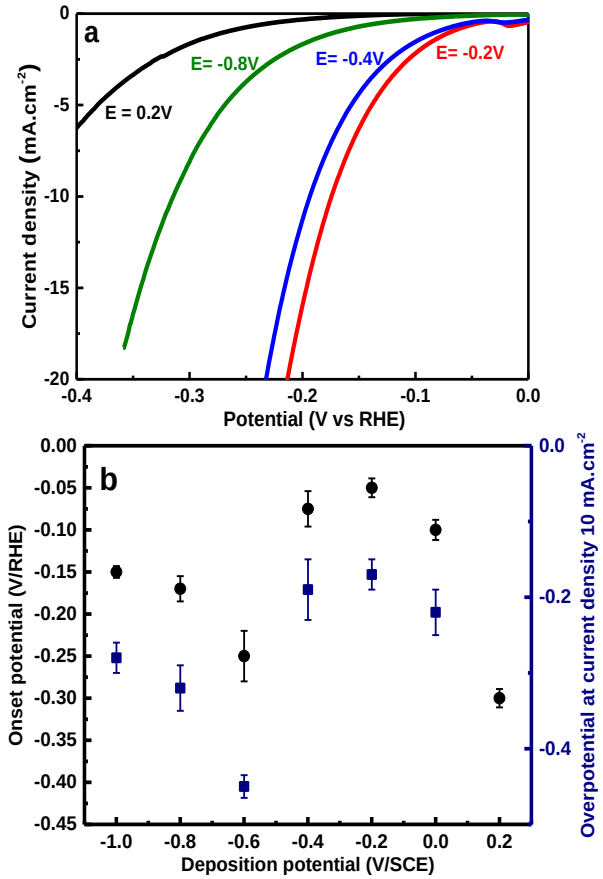

Figure 3. (a) HER polarization curve (LSV) at 10 $mV.s^{-1}$ in 0.5 M H_2SO_4 aqueous solution for GC/Poly(IL)/Pd generated at different electrodeposition potential. (b) Variation of the onset potential (black) and the overpotential (blue) at current density -10 $mA.cm^{-2}$ as function of the deposition potential.

Compared to the bare GC electrode, all the modified electrodes GC/Poly(IL)/Pd NPs exhibit a higher catalytic activity toward HER. The electrocatalytic activity depends on the applied deposition potential, (Figure S3), as attested by the change of the onset potential and the current density. This variation could be related to several parameters including the size and the morphology of the NPs, the exposed active catalyst site, the accessibility to the catalyst and the presence of the polymer brush based ionic liquid. Figure 3b summarizes the electrocatalytic activities of GC/Poly(IL)/Pd NPs generated at different electrodeposition potentials. The curve reports the variation of the onset potential and the required overpotential to achieve a current density -10 $mA.cm^{-2}$ as function of the applied potential for Pd electrodeposition. One has to note that each point represents an average of 5 GC/Poly(IL)/Pd electrodes. The comparison clearly shows that the electrocatalytic activity depends on the applied deposition potential and that the sample prepared at -0.2 V/SCE exhibits the lowest onset potential (-50 mV) and the most positive overpotential (170 mV) at a current density of -10 $mA.cm^{-2}$. In order to evidence the role of the polymer brush

structure, similar experiments were performed by electrodeposition of Pd onto bare GG electrode and their catalytic activities toward HER were evaluated. Figure 4a compares the best electrocatalytic HER performance obtained on the electrodes GC/Pd and GC/Poly(IL)/Pd.

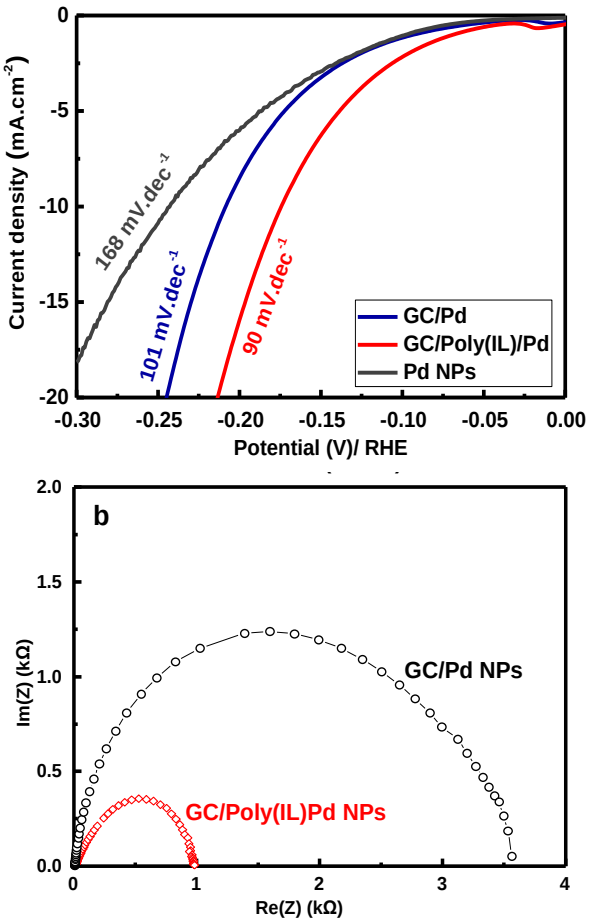

Figure 4. (a) HER polarization curve (LSV) at 10 $mV.s^{-1}$ in 0.5 M H_2SO_4 aqueous solution and the corresponding Tafel slope. (b) EIS curve recorded at -0.2 V/RHE on GC/Pd NPs (black curves) and GC/Poly(IL)/Pd NPs deposited at -0.2 V/ SCE (red curves).

Considering the lowest onset potential and overpotential to achieve -10 $mA.cm^{-2}$, the best electrocatalytic performance was obtained when the Pd is deposited either on GC or GC/Poly(IL) at potential -0.2 V/SCE. The GC/Pd displays an onset potential at -100 mV and an overpotential of about 222 mV, while the GC/Poly(IL)/Pd shows lower values -50 mV for the onset potential and -170 mV for the overpotential. This result suggests that the presence of the poly(IL) enhances the electrocatalytic performance of the Pd toward HER. This enhancement could be related to several parameters including the hierarchical polymer brushes structure that guide the electrochemical growth of the Pd, the chemical composition of the polymer including the presence of nitrogen (electron-rich dopant) in imidazolium which may facilitate the electron transfer and or affect the H* adsorption, and to the presence of synergetic effect between the Pd and the poly(IL).

It is well – known that depending on the catalyst the proton reduction can follow two pathways, the Volmer – Heyrovsky or the Volmer – Tafel mechanism. Being considered as model catalytic reaction, the HER is a typical example of two electron transfer reaction with an intermediate (H* where "*" denotes the catalytic site). The detailed reactions are given below.[45]

Volmer step: $H^+ + e^- + * \rightarrow H^*$ (1)

Heyrovsky step: $H^* + H^+ + e^- \rightarrow H_2 + *$ (2)

Tafel step: $2H^* \rightarrow H_2$ (3)

The reaction rate is largely depended on the adsorption of the proton onto the catalyst surface, i.e. the adsorption free energy (ΔG_H). In the case of low binding energy, the adsorption becomes the rate determining step, RDS, (Volmer step) whereas for strong binding energy, the desorption step becomes the rate determining step (Heyrovsky/Tafel step). To correlate the reaction rate and the mechanism, Tafel slope is used. The value of the Tafel slope determines the RDS. Briefly, Tafel step is the RDS for a Tafel slope around 30 $mV.dec^{-1}$, the value indicating the Heyrovsky step is 40 $mV.dec^{-1}$ and a Tafel slope of 120 $mV.dec^{-1}$ could be attributed to the surface coverage of adsorbed hydrogen or Volmer step.

It is well known that the adsorption of hydrogen into the noble metal lattice results to either the formation of metal hydride surface, called underpotential deposited hydrogen (H-UPD), or overpotential deposited hydrogen, H-OPD, which is generated below H^+/H_2 potential. It has been demonstrated that the H-OPD are intermediates for the reduction reaction while the H-UPD remain spectator during the process.[46] Several works reported that Pd based materials are suitable for hydrogen storage, H-UPD, due to the strong permeability and the high solubility of hydrogen at Pd surface.[47,48] Thus, the adsorption of H-OPD may be the limiting factor for the catalytic performance of the Pd based materials. In our case, values close to 120 $mV.dec^{-1}$ have been obtained for all of the samples (Figure S4a), suggesting that the adsorption of the hydrogen into the catalyst surface is the limiting step. The evolution of the Tafel slope as function of the deposition potential is reported in the Figure S4b. In the absence of the polymeric ionic liquid layer, the GC/Pd NPs shows a Tafel plot around 100 $mV.dec^{-1}$ while The GC/Poly(IL)/Pd NPs exhibits the lowest Tafel slope of 90 $mV.dec^{-1}$, suggesting improvement of the adsorption of the H-OPD. The decrease of the Tafel slope suggests a faster kinetics on GC/Poly(IL)/Pd electrode which could be related to the N (electron-rich dopant in the imidazolium). The latter could induce several effects including, facilitates the efficient electron transfer and reduce the energy barrier. Similar effect has been reported on N doped carbon electrocatalyst.[34,35,49,50] However, the value of the Tafel slope is relatively subjective since the latter depends on the choice of the j-V region and the iR-drop correction. Therefore, the only possible conclusion that can be announced is the exclusion of combination and ion – atom reactions as the limiting steps. Despite the need of more powerful analysis tools for achieving exact mechanism, the clear standpoint is that the electrochemical deposition in the presence of the immobilized ionic liquid

layer enhances the adsorption of hydrogen probably thanks to nitrogen atoms within the imidazolium. This result is further confirmed by the electrochemical impedance spectroscopy tests. As shown in the Figure 4b, the charge transfer resistance is lower in the presence of the polymer ionic liquid layer (1 kΩ compared to 3.5 kΩ), suggesting a higher electron transfer between the catalyst and the electrode surface. Overall, the results confirm that the presence of polymeric ionic liquids influences not only the nano-structuration of the metallic layer but also its catalytic performance.

Even though improvement of the catalytic activity through the presence of PAMI, the performance of the PAMI/Pd is still lower from the activity of platinum. Indeed, similar approach has been performed to Pt based catalysts. The electrochemical deposition was performed onto GC/Poly(IL) electrodes using different deposition potential during 100 s in aqueous electrolytic solution containing Na_2PtCl_4. Afterwards, the catalytic activity of different electrodes was evaluated toward HER in 0.5 M N_2–saturated H_2SO_4 solution as displayed in the Figure 5a and Figure S6.

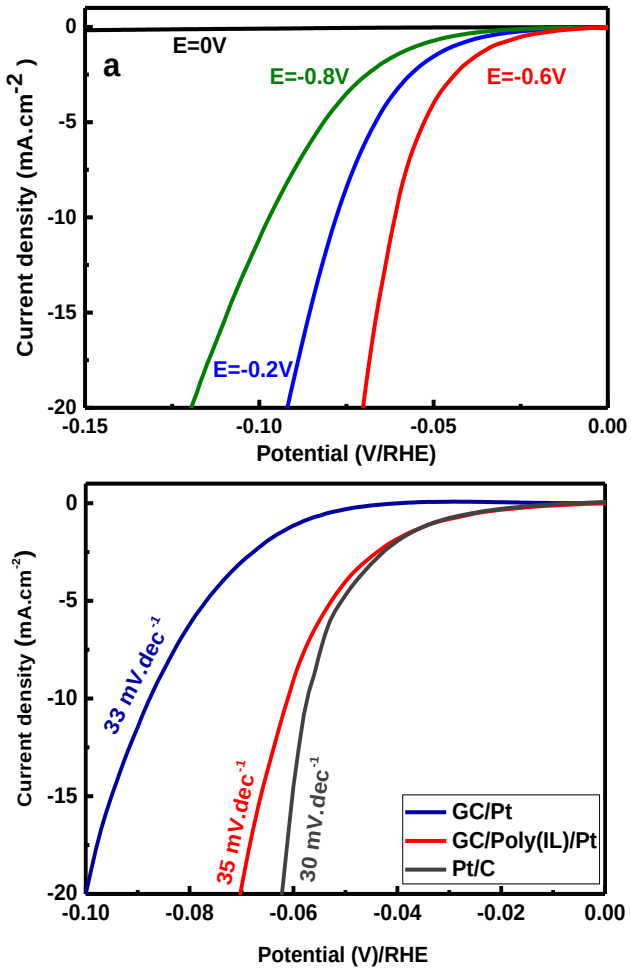

Figure 5. (a) HER polarization curves (LSV) at 10 mV.s^{-1} in 0.5 M H_2SO_4 aqueous solution of GC/Poly(IL)/Pt electrodes obtained at different electrodeposition potential; (b) LSV curves comparing the GC/Pt and GC/Poly(IL)/Pt NPs generated under chronoamperometric conditions at -0.6 V/ SCE.

Figure 5a shows that the electrocatalytic activity of the as-prepared GC/Poly(IL)/Pt toward HER depends on the applied potential during the electrochemical growth of Pt. The comparison displays that the best electrocatalyst with an onset potential at -25 mV corresponds to the sample prepared under amperometric conditions at -0.6 V/ SCE. This sample shows an overpotential of 65 mV to reach 10 mA.cm^{-2}, which is among the most efficient catalysts toward HER.[51-54] Besides that, in the absence of the poly(IL) layer the best GC/Pt electrocatalyst presents onset potential at -55 mV and overpotential of about 90 mV. This result confirms the enhancement of the electrocatalytic activity of noble metal (Pt and Pd) in the presence of polymer ionic liquid, based imidazolium, brush structure.

Next, the Tafel curves were plotted and the slope were calculated for the different generated samples (Figure S5b). The Volmer – Tafel mechanism occurs when the H coverage is very high ($\theta \sim 1$), which is the case for Pt based catalysts.[46] For deposition potential ranging from -0.2 V to -0.8 V/ SCE, the Tafel slopes are found to be around 30 mV.dec^{-1}, indicating that the Tafel step is the rate determining step which is coherent with the previously reported works.[24,55] Interestingly, compared to the activity of the GC/Pt electrode, the presence of polymeric ionic liquid increases the catalytic activity of the platinum (Figure 5b). Indeed, the GC/Poly(IL)/Pt electrode shows a higher catalytic activity with an overpotential of 70 mV to achieve current density of 20 mA.cm^{-2} compared to 100 mV obtained in the absence of the PAMI layer (Figure 5b). Besides, the charge transfer is evaluated using EIS, resulting to a 40-times lower R_{CT} in the case of GC/PAMI/Pt at η = 70 mV. The enhancement of the catalytic performance toward HER confirms the importance of the polymeric ionic liquid. The crucial role of the polymer ionic liquid can be attributed to different features. Firstly, as discussed in the previous part, the concentration of the metallic anion is higher inside the layer rather than in the bulk, suggesting higher nucleation and growth rate due to diffusion-controlled system. Secondly, the organization of the polymer layer in a brush like structure can participate to the orientation of the deposited metallic structure. Finally, the interaction of the polymer layer and the deposited particles may also enhance the hydronium conduction and charge transfer rate at this interface. Another parameter that should be considered is the metal loading (μ). The later was measured using the following formula $\mu = Q \times M/n \times F$, where Q represents the charge during the electrodeposition, M de molecular weight of the metal (Pt or Pd), n the number of electron and F the Faraday constant. The average metal loading in the case of Pd electrodeposited at -0.2 V on GC is 3.6 µg.cm^{-2}, while for Pd deposited onto GC/Poly(IL) a value of 0.4 µg.cm^{-2} was observed. Similarly, in the case of Pt, the estimated metal loading is 5 µg.cm^{-2} for GC/Pt and 0.8 µg.cm^{-2} for GC/Poly(IL)/Pt. Interestingly, the electrochemical deposition of Pd or Pt onto polymer brush ionic liquid leads to decrease the metal loading by a factor of 9 (case of Pd) and 6 (case of Pt) when compared to the electrodeposition on bare GC. Considering this effect the electrocatalytic performances, especially the overpotential

should be lower than the reported values in this work. For a fair comparison, benchmarking catalyst (i.e. commercial Pt/C NPs and Pd NPs) were used. In the case of Pd NPs, the electrochemical deposited nanoparticles exhibit higher catalytic activity compared to the drop-casted Pd NPs. As the particles are support free Pd, this phenomenon could be explained by increasing the charge transfer resistance due to electrical disconnection between particles. Furthermore, based on Marcus – Hush theory, the electron transfer rate constant is related to the reorganization energy and Gibb's free energy. In presence of electron-rich groups, the adsorption of proton could be facilitated, resulting to a decrease of reorganization energy. Thus, the electron transfer rate constant increase. This argument can be solidified by the decrease of the Tafel slope and of charge transfer resistance of Pd NPs in presence of PIL layer, which are obtained from the Figure 4. In contrary, by using Pt as catalyst, the use of PIL to enhance the adsorption of proton could be neglected because the RDS is attributed to the Tafel step. Nevertheless, the presence of PIL provides higher number of nucleation sites for growing of NPs. In case of commercial Pt/C NPs, their activity is slightly higher than our current strategy (Figure 5b). However, it is worth noting that the metal loading is about 60 times lower by using electrodeposition (0.8 $\mu g.cm^{-2}$ vs 46 $\mu g.cm^{-2}$), suggesting an increase of catalytic performance in terms of normalized metal loading.

Indirect electrochemical deposition approach. The purpose of this part is to prove the possibility to generate nanoclusters of noble metal by the anion capturing property of the polymeric ionic liquid, e.g. poly(1-allyl-3-methylimidazolium). The imidazolium skeleton of the as-prepared poly(IL) film creates extremely high cationic charge density at the interface between the electrode/solution interface. The electrostatic attraction allows strong molecular interaction between the imidazolium rings and metal-based anion ($PdCl_4^{2-}$). The specific feature allows the PAMI modified electrode receiving a large density of metal precursors, which acts as reservoir for further electrochemical deposition of clusters.

The electrochemical nucleation and growth of the nanoparticles can be occurred in distilled water under self-electrolytic conditions (without any additional supporting electrolyte). The electrochemistry of immobilized ionic liquid in electrolytic free solution is reported in the previous works.[56,57] Thus, by applying a cathodic potential, the anion ($PdCl_4^{2-}$) inside the film can act as both precursor and metal reservoir for growing the nanoparticles. After the electrochemical deposition in aqueous solution, the presence of clusters was first evidenced by the electrochemical characterization in aqueous acidic solution (0.5 M H_2SO_4). The typical signal of the Pd^0 (Figure S6) was observed as described in the previous part. However, the current intensity attributed to the oxidation of Pd and Pt particles is lower than that observed for direct approach. It is noted that even the concentration at the vicinity of the electrode is higher in the current case, the quantity of the anions is still scanty within very thin layer of the polymer. Thus, the quantity of metallic Pd generated in this case must be lower.

X-ray photoelectron spectroscopy (XPS) was used to follow the change in the chemical composition of the surface of different substrates (Figure 6).

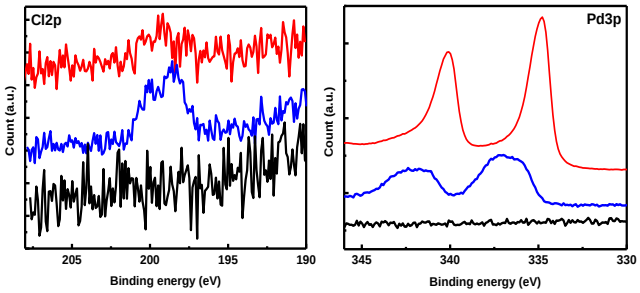

Figure 6. High resolution XPS spectra of Cl(2p) and Pd(3p), elements on different substrates. (Black curves) GC/Poly(IL), (blue curves) GC/ Poly(IL)/$PdCl_4^{2-}$ and (red curves) GC/ Poly(IL)/$Pd_{indirect}$.

After anion exchange, the high-resolution spectra of the Pd(3p) exhibits lump signal of the Pd^{2+} ($3p^{3/2}$ and $3p^{1/2}$) centered at 337 eV and 343 eV, indicating the presence of $PdCl_4^{2-}$ within the polymer film (blue curve Figure 6). Interestingly, after the electrochemical deposition, the Pd(3p) peaks are shifted to lower binding energy 334.8 eV and 340.8 eV corresponding to Pd^0 confirming the formation of metallic Pd inside the polymeric film (red curve Figure 6). The binding energy of Pd^0 is shifted by 0.25 eV compared to bare metallic Pd. The latter is attributed to a strong interaction between metallic Pd and nitrogen atoms from the polymer layer. Consequently, the Pd particles have negative charge when they are in contact with the film, leading to higher catalytic performance[58]. In addition, the variation of the Cl(2p) signals confirms the occurrence of the anion exchange. Precisely, the appearance of Cl signal at 198 eV and 199 eV, attributed to $2p_{3/2}$ and $2p_{1/2}$ respectively, confirms that the $PdCl_4^{2-}$ is trapped inside the polymer layer (blue curve Figure 6). Next, a decrease of the Cl^- contribution after the electrodeposition (red curve Figure 6) is observed confirming the formation of metallic Pd. Moreover, the nitrogen signal at 401.5 eV is still visible confirming the presence of imidazolium. Overall, the XPS measurements evidence the anion exchange and the presence of metallic Pd generated after electrochemical treatment in aqueous electrolyte free solution.

Afterwards, the catalytic performance of the as-prepared electrodes toward the HER was evaluated. Figure S7a displays the LSV of different GC/Poly(IL)/$Pd_{indirect}$ electrodes generated under various potential deposition. The comparison clearly shows the presence of electrocatalytic activity and that the sample prepared under a cathodic electrodeposition at -0.2 V/SCE exhibits the highest performance. Typically, the GC/Poly(IL)/$Pd_{indirect}$ deposited at -0.2 V/SCE exhibits the lowest onset potential around -100 mV and an overpotential of 240 mV for a current density about -10 $mA.cm^{-2}$ (Figure 7a). It is known that the electrocatalytic property of a material is influenced by several factors, including electrical conductivity, defect

density, electrochemical active surface area (ECSA) of the material, etc. The value of ECSA was calculated according to the following equation (2):

$$ECSA\,(m^2.g^{-1}) = \frac{Q_H}{WAQ_{H-M}} x10^6 \qquad (2)$$

Where W is the quantity of metal loading (μg.cm^{-2}), A is the geometric surface area of electrode (cm^2), Q_H (C) is the electric charge for hydrogen adsorption/desorption and $Q_{H\text{-}M}$ (C.m^{-2}) is the standard charge of hydrogen on a smooth metal M surface.

The ECSA for Pd generated using the indirect approach provides higher ECSA (55.47) compared to the direct electrochemical deposition approach (2-3 times). X. Xie et al reported the ECSA value of 51.17 m^2.g^{-1} for 5-7 nm reduced-polyoxometalate supported palladium which is lower than our reported value, confirming that the generated particles via indirect approach have smaller size than 5 nm.[57] The stability of the GC/Poly(IL)/Pd$_{indirect}$ electrode was tested as shown in Figure S8). The result displays that the current retention remains higher than 90 % after a polarization at – 0.2 V vs RHE during 4000 s.

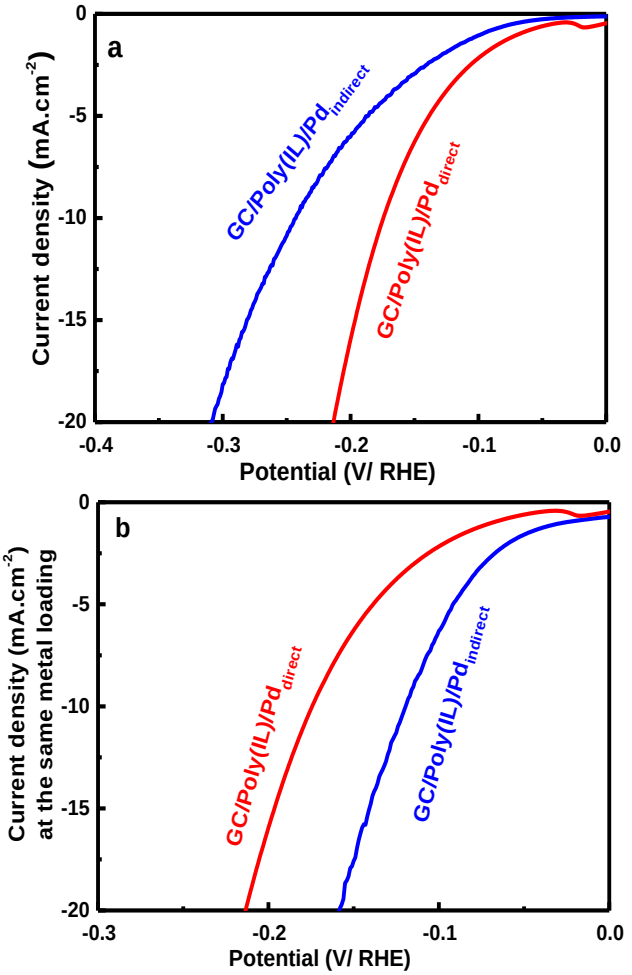

Figure 7. (a) HER polarization curve at 10 mV.s^{-1} in 0.5 M H_2SO_4 aqueous solution on GC/Poly(IL)/Pd$_{direct}$ (red) and GC/Poly(IL)/Pd$_{indirect}$ (blue). (b) Variation of the current density at the same metal loading as function of the potential.

The kinetic is evaluated by plotting the Tafel curve which gives a value of 89 mV.dec^{-1}, indicating a higher adsorption rate by decreasing Volmer step limitation (Figure S7b). This value is similar to that obtained from the direct approach, suggesting both samples follow the same HER mechanism. To get more insight about the charge transfer kinetic, electrochemical impedance spectroscopy was performed at different overpotential for the sample prepared at -0.2 V/ SCE (Figure S9). As displayed in the Figure S8a, the GC/PAMI/Pd$_{indirect}$ exhibits single semicircle for all of the used overpotentials, suggesting that the equivalent circuit can be constructed by single time constant. The potential dependence of the resistance and of the capacitance (R-CPE circuit) reflects the kinetic of the HER process. Indeed, the charge transfer resistance decreases from 8250 Ω at η = 60 mV to 500 Ω at η = 200 mV. In addition, the variation of the log(R_{CT}^{-1}) as function of the overpotential was plotted as shown in the Figure S8c, resulting to a linear relationship at low overpotential. The calculated Tafel slope is 83 mV.dec^{-1} for the GC/Poly(IL)/Pd$_{indirect}$ obtained from the EIS data which is similar to that obtained from the LSV. In addition to the value of the charge transfer resistance, the capacitance derived from the CPE is another important parameter. The application of high overpotential conducts to a decrease of the double layer capacitance (Figure S9e) from 0.14 mF.cm^{-2} at 60 mV (approximately 40 mF.mg^{-1}) to 0.04 mF.cm^{-2} at 200 mV (~15 mF.mg^{-1}). These variations could be attributed to the partial blockage of the electrode surface by the generated hydrogen species due to the formation of microbubbles. The high values of the double layer capacitance for the particles decorated the polymer ionic liquids highlight the ionic character of the polymer and the small size of the particles, suggesting the presence of large specific surface areas. Besides, the time constant for the electron transfer across the catalyst/electrolyte interface can be estimated as, i.e. τ = RC, where smaller τ represents higher electron transfer rate. As presented in the Figure S8d, the evolution of τ as function of the potential shows a decrease by 3 orders of magnitude from 0 V to -0.17 V/RHE, suggesting an increase of the electron transfer kinetic. In addition, below -0.2 V/RHE, τ values reach saturation at around (10^{-3} s). This value reflects purely the charge transfer kinetic and excludes other contributions suggesting that the Volmer step is the RDS during the reduction process.

In the other hand, the overpotential needed to reach -10 mA.cm^{-2} at the GC/Poly(IL)/Pd$_{indirect}$ is around 240 mV compared to 222 and 170 mV obtained for GC/Pd NPs and GC/Poly(IL)/Pd$_{direct}$, respectively. A simple comparison may lead to conclude that the GC/Poly(IL)/Pd$_{indirect}$ electrode presents a better electrocatalytic performance when compared to GC/Poly(IL)/Pd$_{indirect}$. However, as stated above the quantity of the metal within the film has to be considered for a more accurate evaluation of the electrocatalytic performance. Thus, the sample prepared via ion exchange approach is a promising route to decrease the quantity of the active materials. Indeed, the metal loading of Pd using the indirect approach is around 0.04 μg.cm^{-2} which is 1 order of magnitude lower than that measured

for a direct approach (0.4 $\mu g.cm^{-2}$) and almost 2 orders of magnitude lower when compared to GC/Pd sample (3.6 $\mu g.cm^{-2}$). Indeed, considering this difference, the LSV curves were replotted by reporting the variation of the current density at the same metal loading as function of the potential (Figure 7b). Taking onto account this parameter the onset is -25 mV and the overpotential to reach -10 $mA.cm^{-2}$ is 120 mV. As consequence, the GC/Poly(IL)/$Pd_{indirect}$ displays a higher electrocatalytic performance toward HER when compared to GC/Poly(IL)/Pd_{direct} and GC/Pd.

■ CONCLUSION

In summary, this work investigates the electrochemical deposition of Pt and Pd onto polymer brush ionic liquid based on imidazolium. A series of hybrid materials generated using direct electrochemical deposition over the polymer layer were investigated. The presence of the polymer layer changes the morphology of the electrodeposited nanoparticles. Thus, the hybrid materials exhibit an enhancement of the catalytic performance. In a second approach, the polymer ionic liquid is used as a host -guest platform to capture the metallic anion, followed by electrochemical deposition under self-electrolytic condition in distilled water. The final hybrid material displays a strong electrocatalytic activity toward HER with a low catalyst loading (up to 2 orders of magnitude). The presented approach could be extended to other monomer ionic liquid, metals and transition metals dichalcogenides such as MoS_2. The simplicity of the material elaboration combined to the number of possible polymer-based ionic liquids (estimated around 10^4 polymers) is a promising route toward the modulation of the catalytic performance of metal electrocatalysts.

ASSOCIATED CONTENT

Supporting Information.
This material is available free of charge via the Internet at http://pubs.acs.org.
HER evaluation in function of deposition potential and calculated Tafel slope for 2 approaches.

AUTHOR INFORMATION

Corresponding Author

* Jalal Ghilane.
Email: jalal.ghilane@univ-paris-diderot.fr

Notes

Authors declare no competing financial interest

ACKNOWLEDGMENT

The authors thank Dr. Philippe Decorse for XPS measurements. T.N. Pham-Truong acknowledge Doctoral School ED388 for Ph.D. grant. ANR (Agence Nationale de la Recherche) and CGI (Commissariat à l'Investissement d'Avenir) are gratefully acknowledged for their financial support of this work through Labex SEAM (Science and Engineering for Advanced Materials and devices) ANR 11-LABX-086, ANR-11-IDEX-05-02.

REFERENCES

(1) Jiao, Y.; Zheng, Y.; Jaroniec, M.; Qiao, S.Z. Design of Electrocatalysts for Oxygen- and Hydrogen-Involving Energy Conversion Reactions. *Chem. Soc. Rev.* **2015**, *44*, 2060–2086.

(2) Guo, Y.; Tang, J.; Henzie, J.; Jiang, B.; Qian, H.; Wang, Z.; Tan, H.; Bando, Y.; Yamauchi, Y. Assembly of Hollow Mesoporous Nanoarchitectures Composed of Ultrafine Mo2C Nanoparticles on N-doped Carbon Nanosheets for Efficient Electrocatalytic Reduction of Oxygen. *Mater. Horiz.* **2017**, *4*, 1171-1177.

(3) Tan, H.; Tang, J.; Henzie, J.; Li, Y.; Xu, X.; Chen, T.; Wang, Z.; Wang, J.; Ide, Y.; Bando, Y.; Yamauchi, Y. Assembly of Hollow Carbon Nanospheres on Graphene Nanosheets and Creation of Iron–Nitrogen-Doped Porous Carbon for Oxygen Reduction. *ACS Nano*, **2018**, *12*, 5674–5683.

(4) (4) Tan, H.; Li, Y.; Kim, J.; Takei, T.; Wang, Z.; Xu, X.; Wang, J.; Bando, Y.; Kang, Y-M.; Tang, J.; Yamauchi, Y. Sub-50 nm Iron–Nitrogen-Doped Hollow Carbon Sphere-Encapsulated Iron Carbide Nanoparticles as Efficient Oxygen Reduction Catalysts. *Adv Sci*, **2018**, *5*, 1800120.

(5) Guo,Y.; Park, T.; Yi, J.W.; Henzie, J.; Kim, J.; Wang, Z.; Jiang, B.; Bando, Y.; Sugahara, Y.; Tang, J.; Yamauchi, Y. Nanoarchitectonics for Transition-Metal-Sulfide-Based Electrocatalysts for Water Splitting. *Adv Mater*, **2019**, *31*, 1807134.

(6) Tang, K.; Wang, X.; Li, Q.; Yan, C. High Edge Selectivity of In Situ Electrochemical Pt Deposition on Edge-Rich Layered WS_2 Nanosheets. *Adv. Mater.* **2018**, *30*, 1704779.

(7) Chen, H.; Wei, G.; Ispas, A.; Hickey, S.G.; Eychmüller, A. Synthesis of Palladium Nanoparticles and Their Applications for Surface-Enhanced Raman Scattering and Electrocatalysis. *J. Phys. Chem. C* **2010**, *114* , 21976–21981.

(8) Zheng, J.; Zhou, S.; Gu, S.; Xu, B.; Yan, Y. Size-Dependent Hydrogen Oxidation and Evolution Activities on Supported Palladium Nanoparticles in Acid and Base. *J. Electrochem. Soc.* **2016**, *163*, F499–F506.

(9) Xu, D.; Liu, X.; Lv, H.; Liu, Y.; Zhao, S.; Han, M.; Bao, J.; He, J.; Liu, B. Ultrathin Palladium Nanosheets with Selectively Controlled Surface Facets. *Chem. Sci*. **2018**, *9*, 4451–4455.

(10) Xu, D.; Lv, H.; Jin, H.; Liu Y.; Ma, Y.; Han, M.; Bao, J.; Liu, B. Crystalline Facet-Directed Generation Engineering of Ultrathin Platinum Nanodendrites. *J. Phys. Chem. Lett.* **2019**, *103*, 663–671.

(11) Popczun, E.J.; Read, C.G.; Roske, C.W.; Lewis, N.S.; Schaak, R.E. Highly Active Electrocatalysis of the Hydrogen Evolution Reaction by Cobalt Phosphide Nanoparticles. *Angew. Chem., Int. Ed.* **2014**, *53*, 5427–5430.

(12) Popczun, E.J.; McKone, J.R.; Read, C.G.; Biacchi, A. J.; Wiltrout, A.M.; Lewis, N.S.; Schaak, R.E. Nanostructured Nickel Phosphide as an Electrocatalyst for the Hydrogen Evolution Reaction. *J. Am. Chem. Soc.* **2013**, *135*, 9267–9270.

(13) Li, Y.; Wang, H.; Xie, L.; Liang, Y.; Hong, G.; Dai, H. MoS_2 Nanoparticles Grown on Graphene: An Advanced Catalyst for the Hydrogen Evolution Reaction. *J. Am. Chem. Soc.* **2011**, *133*, 7296–7299.

(14) Zhang, J.; Qu, L.; Shi, G.; Liu, J.; Chen, J.; Dai, L. N,P-Codoped Carbon Networks as Efficient Metal-free Bifunctional Catalysts for Oxygen Reduction and Hydrogen Evolution Reactions. *Angew. Chem., Int. Ed.* **2016**, *55*, 2230–2234.

(15) Wang, X.; Maeda, K.; Chen, X.; Takanabe, K.; Domen, K.; Hou, Y.; Fu, X.; Antonietti, M. Polymer Semiconductors for Artificial Photosynthesis: Hydrogen Evolution by Mesoporous Graphitic Carbon Nitride with Visible Light. *J. Am. Chem. Soc.* **2009**, *131*, 1680–1681.

(16) Zheng, Y.; Jiao, Y.; Zhu, Y.; Li, L. H.; Han, Y.; Chen, Y.; Du, A.; Jaroniec, M.; Qiao, S. Z. Hydrogen Evolution by a Metal-Free Electrocatalyst. *Nat. Commun.* **2014**, *5*, 3783.

(17) Wang, X.; Maeda, K.; Thomas, A.; Takanabe, K.; Xin, G.; Carlsson, J. M.; Domen, K.; Antonietti, M. A Metal-Free Polymeric

Photocatalyst for Hydrogen Production from Water Under Visible Light. *Nat. Mater.* **2009**, *8*, 76–80.

(18) Yin, H.; Zhao, S.; Zhao, K.; Muqsit, A.; Tang, H.; Chang, L.; Zhao, H.; Gao, Y.; Tang, Z. Ultrathin Platinum Nanowires Grown on Single-Layered Nickel Hydroxide with High Hydrogen Evolution Activity. *Nat. Commun*. **2015**, *6*, 6430.

(19) Sarkar, S.; Peter, S. C. An Overview on Pd-Based Eectrocatalysts for the Hydrogen Evolution Reaction. *Inorg. Chem. Front*. **2018**, *5*, 2060–2080.

(20) Wang, D.Y.; Gong, M.; Chou, H.L.; Pan, C.J.; Chen, H.A.; Wu, Y.; Lin, M.C.; Guan, M.; Yang, J.; Chen, C.W.; Wang, Y.L.; Hwang, B.J.; Chen, C.C.; Dai, H. Highly Active and Stable Hybrid Catalyst of Cobalt-Doped FeS_2 Nanosheets–Carbon Nanotubes for Hydrogen Evolution Reaction. *J. Am. Chem. Soc*. **2015**, *137*, 41587–1592.

(21) Wang, S.; Wang, J.; Zhu, M.; Bao, X.; Xiao, B.; Su, D.; Li, H.; Wang, Y. Molybdenum-Carbide-Modified Nitrogen-Doped Carbon Vesicle Encapsulating Nickel Nanoparticles: A Highly Efficient, Low-Cost Catalyst for Hydrogen Evolution Reaction. *J. Am. Chem. Soc*. **2015**, *137*, 15753-15759

(22) Lin, L.; Zhou, W.; Gao, R.; Yao, S.; Zhang, X.; Xu, W.; Zheng, S.; Jiang, Z. Yu, Q.; Li, Y.W.; Shi, C.; Wen X.D.; Ma, D. Low-Temperature Hydrogen Production from Water and Methanol using Pt/α-MoC Catalysts. *Nature* **2017**, *544*, 80–83

(23) Chao, T.; Luo, X.; Chen, W.; Jiang, B.; Ge, J.; Lin, Y.; Wu, G.; Wang, X.; Hu, Y.; Zhuang, Z.; Wu, Y.; Hong, X.; Li, Y. Atomically Dispersed Copper-Platinum Dual Sites Alloyed with Palladium Nanorings Catalyze the Hydrogen Evolution Reaction. *Angew. Chem., Int. Ed*. **2017**, *56*, 16047–16051.

(24) Cheng, N.; Stambula, S.; Wang, D.; Banis, M. N.; Liu, J.; Riese, A.; Xiao, B.; Li, R.; Sham, T. K.; Liu, L. M.; Botton, G. A.; Sun, X. Platinum Single-Atom and Cluster Catalysis of the Hydrogen Evolution Reaction. *Nat. Commun*. **2016**, *7*, 13638.

(25) Zhang, L.; Han, L.; Liu, H.; Liu, X.; Luo, J. Potential-Cycling Synthesis of Single Platinum Atoms for Efficient Hydrogen Evolution in Neutral Media. *Angew. Chem., Int. Ed*. **2017**, *56*, 13694–13698.

(26) Du, Y.; Sheng, H.; Astruc, D.; Zhu, M. Atomically Precise Noble Metal Nanoclusters as Efficient Catalysts: A Bridge between Structure and Properties. *Chem. Rev*. **2019**, https://doi.org/10.1021/acs.chemrev.8b00726

(27) Zhang, G.R.; Etzold, B. J. M. Ionic Liquids in Electrocatalysis. *J. Energy Chem*. **2016**, *25*, 199–207.

(28) Qiu, B.; Lin, B.; Yan, F. Ionic Liquid/Poly(Ionic Liquid)-Based Electrolytes for Energy Devices. *Polym. Int*. **2013**, *62*, 335–337.

(29) Watanabe, M.; Thomas, O.L.; Zhang, S.; Ueno, K.; Yasuda, T.; Dokko, K. Application of Ionic Liquids to Energy Storage and Conversion Materials and Devices. *Chem. Rev.* **2017**, *117*, 7190–7239.

(30) Tokuda, H.; Hayamizu, K.; Ishii, K.; Susan, M.A.B.H.; Watanabe, M. Physicochemical Properties and Structures of Room Temperature Ionic Liquids. 2. Variation of Alkyl Chain Length in Imidazolium Cation. *J. Phys. Chem*. B **2005**, *109*, 6103–6110.

(31) Zhao, X.; Li, S.; Cheng, H.; Schmidt, J.; Thomas, A. Ionic Liquid-Assisted Synthesis of Mesoporous Carbons with Surface-Enriched Nitrogen for the Hydrogen Evolution Reaction. *ACS Appl. Mater. Interfaces* **2018**, *10*, 3912–3920.

(32) Wallace, A. G.; Symes, M. D. Water-Splitting Electrocatalysts Synthesized Using Ionic Liquids. *Trends in Chemistry* **2019**, *1*, 247–258.

(33) Zhang, B.; Xue, Y.; Jiang, A.; Xue, Z.; Li, Z.; Hao, J. Ionic Liquid as Reaction Medium for Synthesis of Hierarchically Structured One-Dimensional MoO_2 for Efficient Hydrogen Evolution. *ACS Appl. Mater. Interfaces* **2017**, *9*, 7217–7223.

(34) Martinaiou, I.; Wolker, T.; Shahraei, A.; Zhang, G.R.; Janßen, A.; Wagner, S.; Weidler, N.; Stark, R.W.; Etzold, B.J.M.; Kramm, U.I. Improved Electrochemical Performance of Fe-N-C Catalysts Through Ionic Liquid Modification in Alkaline Media. *Journal of Power Sources* **2018**, *375*, 222–232.

(35) Snyder, J.; Fujita, T.; Chen, M.W.; Erlebacher, J. Oxygen Reduction in Nanoporous Metal–Ionic Liquid Composite Electrocatalysts. *Nature Mater*. **2010**, *9*, 904–907

(36) Pham Truong, T. N.; Randriamahazaka, H.; Ghilane, J. Polymer Brushes Ionic Liquid as a Catalyst for Oxygen Reduction and Oxygen Evolution Reactions. *ACS Catal*. **2018**, *8*, 869–875.

(37) Pham Truong, T. N.; Ranjan, C.; Randriamahazaka, H.; Ghilane, J. Nitrogen Doped Carbon Dots Embedded in Poly(Ionic Liquid) as High Efficient Metal-Free Electrocatalyst for Oxygen Reduction Reaction. *Catal. Today* **2019**, *335*, 381–387.

(38) Milchev, A. Electrochemical Phase Formation on a Foreign Substrate—Basic Theoretical Concepts and Some Experimental Results. *Contemp. Phys*. **1991**, *32*, 321–332.

(39) Palomar-Pardavé, M.; González, I.; Batina, N. New Insights into Evaluation of Kinetic Parameters for Potentiostatic Metal Deposition with Underpotential and Overpotential Deposition Processes. *J. Phys. Chem. B* **2000**, *104*, 3545–3555.

(40) Rezaei, M.; Tabaian, S.H.; Haghshenas, D.F. Nucleation and Growth of Pd Nanoparticles during Electrocrystallization on Pencil Graphite. *Electrochim. Acta* **2012**, *59*, 360–366.

(41) Bui-Thi-Tuyet, V.; Trippé-Allard, G.; Ghilane, J.; Rriamahazaka, H. Surface and Electrochemical Properties of Polymer Brush-Based Redox Poly(Ionic Liquid). *ACS Appl. Mater. Interfaces*, **2016**, *8*, 28316–28324.

(42) Bouden, S.; Gómez-Mingot, M.; Randriamahazaka, H.; Ghilane, J. Surface Initiated Immobilization of Molecules Contained in an Ionic Liquid Framework. *Anal. Chem*. **2016**, *88*, 1017–1021.

(43) Chen, L.; Yelon, A.; Sacher, A. X-ray Photoelectron Spectroscopic Studies of Pd Nanoparticles Deposited onto Highly Oriented Pyrolytic Graphite: Interfacial Interaction, Spectral Asymmetry, and Size Determination. *J. Phys. Chem. C* **2011**, *115*, 7896–7905.

(44) Ghilane, J.; Lacroix, J.C. Formation of a Bifunctional Redox System Using Electrochemical Reduction of Platinum in Ferrocene Based Ionic Liquid and Its Reactivity with Aryldiazonium. *J. Am. Chem. Soc*. **2013**, *135*, 4722–4728.

(45) Sun, H.; Xu, X.; Yan, Z.; Chen, X.; Cheng, F.; Weiss, P.S.; Chen, J. Porous Multishelled Ni_2P Hollow Microspheres as an Active Electrocatalyst for Hydrogen and Oxygen Evolution. *Chem. Mater*. **2017**, *29*, 8539-8547.

(46) Conway, B.E.; Tilak, B.V. Interfacial Processes Involving Electrocatalytic Evolution and Oxidation of H_2 and the Role of Chemisorbed H. *Electrochim. Acta* **2002**, *47*, 3571–3594.

(47) Green, T.; Britz, D. Kinetics of the Deuterium and Hydrogen Evolution Reactions at Palladium in Alkaline Solution. *J. Electroanal. Chem*. **1996**, *412*, 59–66.

(48) Zalineeva, A.; Baranton, S.; Coutanceau, C.; Jerkiewicz, G. Octahedral Palladium Nanoparticles as Excellent Hosts for Electrochemically Adsorbed and Absorbed Hydrogen. *Sci. Adv*. **2017**, *3*, e1600542.

(49) Li, D.J.; Maiti, U.N.; Lim, J.; Choi, D.S.; Lee, W.J.; Oh, Y.; Lee, G.Y.; Kim, S.O. Molybdenum Sulfide/N-Doped CNT Forest Hybrid Catalysts for High-Performance Hydrogen Evolution Reaction. *Nano Lett*. **2014**, *14*, 1228–1233.

(50) Zheng, Y.; Jiao, Y.; Li, L.H.; Xing, T.; Chen, Y.; Jaroniec, M.; Qiao, S.Z. Toward Design of Synergistically Active Carbon-Based Catalysts for Electrocatalytic Hydrogen Evolution. *ACS Nano* **2014**, *8*, 5290–5296

(51) Dasgupta, N.P.; Liu, C.; Andrews, S.; Prinz, F.B.; Yang, P. Atomic Layer Deposition of Platinum Catalysts on Nanowire Surfaces for Photoelectrochemical Water Reduction. *J. Am. Chem. Soc*. **2013**, *135*, 12932–12935.

(52) Raoof, J. B.; Ojani, R.; Kiani, A.; Rashid-Nadimi, S. Fabrication of Highly Porous Pt Coated Nanostructured Cu-Foam Modified Copper Electrode and its Enhanced Catalytic Ability for Hydrogen Evolution Reaction. *Int. J. Hydrogen Energy* **2010**, *35*, 452–458.

(53) Begum, H.; Ahmed, M.S.; Jeon, S. Highly Efficient Dual Active Palladium Nanonetwork Electrocatalyst for Ethanol Oxidation and Hydrogen Evolution. *ACS Appl. Mater. Interfaces* **2017**, *9*, 39303–39311.

(54) Wang, P.; Zhang, X.; Zhang, J.; Wan, S.; Guo, S.; Lu, G.; Yao, J.; Huang, X. Precise Tuning in Platinum-Nickel/Nickel Sulfide Interface Nanowires for Synergistic Hydrogen Evolution Catalysis. *Nat. Commun*. **2017**, *8*, 14580.

(55) Li, K.; Li, Y.; Wang, Y.; Ge, J.; Liu, C.; Xing, W. Enhanced Electrocatalytic Performance for the Hydrogen Evolution Reaction Through Surface Enrichment of Platinum Nanoclusters Alloying with Ruthenium In Situ Embedded in Carbon. *Energy Environ. Sci*. **2018**, *11*, 1232–1239.

(56) Pham Truong, T. N.; Randriamahazaka, H.; Ghilane, J. Redox Monomer Ionic Liquid Based on Quaternary Ammonium: From Electrochemistry to Polymer Brushes. *Electrochem. commun*. **2017**, *82*, 25–29.

(57) Bui-Thi-Tuyet, V.; Trippe-Allard, G.; Ghilane, J.; Randriamahazaka, H. Surface and Electrochemical Properties of Polymer Brush-Based Redox Poly(Ionic Liquid). ACS Appl. Mater. Interfaces **2016**, *8*, 28316–28324.

(58) Liu, B.; Wang, P.; Lopes, A.; Jin, L.; Zhong, W.; Pei, Y.; Suib, S. L.; He, J., Au–Carbon Electronic Interaction Mediated Selective Oxidation of Styrene. ACS Catal. **2017**, 7, 3483–3488.

(59) Xie, X.; Nie, Y.; Chen, S.; Ding, W.; Qi, X.; Li, L.; Wei, Z. A Catalyst Superior to Carbon-Supported-Platinum for Promotion of the Oxygen Reduction Reaction: Reduced-Polyoxometalate Supported Palladium. *J. Mater. Chem. A* **2015**, *3*, 13962–13969.